Journal of Solid State Chemistry 181 (2008) 3037–3043

Contents lists available at ScienceDirect

Journal of Solid State Chemistry

journal homepage: www.elsevier.com/locate/jssc

An ab initio study of possible pathways in the thermal decomposition of $NaAlH_4$

J.G.O. Ojwang [a,*], Rutger van Santen [a], Gert Jan Kramer [a], Xuezhi Ke [b]

[a] Schuit Institute of Catalysis, Eindhoven University of Technology, Postbus 513, 5600 MB, Den Dolech 2, Eindhoven, The Netherlands
[b] Department of Physics, East China Normal University, Shanghai 200062, China

ARTICLE INFO

Article history:
Received 18 March 2008
Received in revised form
21 July 2008
Accepted 4 August 2008
Available online 17 August 2008

Keywords:
Hydrogen storage
Crystals
Heats of formation

ABSTRACT

Density functional theory (DFT) has been used to study the structural stability of possible intermediate alanate structures, $Na_5Al_3H_{14}$ and Na_2AlH_5, in the thermal decomposition of $NaAlH_4$. $Na_5Al_3H_{14}$ crystallizes in the space group $P4/mnc$ with lattice constants $a = 6.769$ A , $c = 10.289$ A and $c/a = 1.52$. It is shown that both $Na_5Al_3H_{14}$ and Na_2AlH_5 have the right thermodynamics and can fit in as an intermediate state during the thermal decomposition process of $NaAlH_4$. The heat of formation of $Na_5Al_3H_{14}$ is -60 kJ/mol H_2, which is intermediate between that of $NaAlH_4$ (-51 kJ/mol H_2) and Na_3AlH_6 (-69.7 kJ/mol H_2). An alternative decomposition pathway based on Na_2AlH_5 has also been discussed. Frequency analysis showed that the least energetic Na_2AlH_5 structure has imaginary frequencies, implying that it is unstable. The presence of soft phonon modes also shows that $Na_5Al_3H_{14}$ is mechanically metastable. These results are consistent with the notion that they are the intermediate states that lead to the formation of AlH_3. This facilitates the mass transport of aluminum atoms in the decomposition pathway of $NaAlH_4$.

1. Introduction

Complex metal hydrides have generated much interest as candidates for hydrogen storage due to their relatively high weight percent of hydrogen and favorable thermodynamics like in the case of $NaAlH_4$ [1–10]. The different phases that are formed during the thermal decomposition of $NaAlH_4$ have already been experimentally identified. However, the detailed transformation chemistry of the thermal decomposition of $NaAlH_4$ is not yet fully understood. Based on experimental observations the putative desorption pathway is as follows:

$$NaAlH_4 \leftrightarrow \tfrac{1}{3}Na_3AlH_6 + \tfrac{2}{3}Al + H_2 \quad (1)$$

$$Na_3AlH_6 \leftrightarrow 3NaH + Al + \tfrac{3}{2}H_2 \quad (2)$$

It has, however, been noted that although Na_3AlH_6 is an experimentally established intermediate phase the reaction does not necessarily proceed via the above pathway (Eqs. (1) and (2)) [5] since it cannot explain how the long range mass transport of metallic Al species takes place. It is possible that there are many other sub-intermediate paths, with Na_3AlH_6 as an observable intermediate product. It is now generally accepted that aluminum hydride might play a key role in the mass transport of aluminum atoms [5,11,12]. Fu et al. [11] have shown, using inelastic neutron scattering, that indeed AlH_3 species might be present during the decomposition of titanium-doped $NaAlH_4$. Gross et al. did an in situ X-ray diffraction study of the decomposition of $NaAlH_4$ and found that there were some unidentified intermediate phases, X_1 and X_2, during the process of decomposition [5]. They were, however, not able to determine the crystal structure of these phases. In order to rationalize the fact that a surface catalyst influences a bulk transition they suggested that a better way to understand the thermal decomposition of $NaAlH_4$ is to reformulate the reaction:

$$NaAlH_4 \leftrightarrow \tfrac{1}{3}Na_3AlH_6 + \tfrac{2}{3}Al + H_2 \leftrightarrow NaH + Al + \tfrac{3}{2}H_2 \quad (3)$$

into

$$3(NaH)(AlH_3) \leftrightarrow (NaH)_3(AlH_3) + 2(AlH_3) \leftrightarrow 3(NaH) + 3(AlH_3) \quad (4)$$

so that the phase transitions in Eq. (1) is caused by the molecular movements of AlH_3 and NaH species. The support for this model of Gross is based on the fact that $NaAlH_4$ can be indirectly synthesized by mixing Na_3AlH_6 [13] or NaH [14] with AlH_3 in tetrahydrofuran. The mobile AlH_3 species acts as the vessels through which the Al is transported in the system. The key question is how is AlH_3 formed? In an attempt to answer this question, Walters and Scogin [15] proposed the following

* Corresponding author.
E-mail address: j.g.o.ojwang@tue.nl (J.G.O. Ojwang).

0022-4596/$ - see front matter © 2008 Elsevier Inc. All rights reserved.
doi:10.1016/j.jssc.2008.08.010

reaction pathway:

$$NaAlH_4 \leftrightarrow NaH + AlH_3 \quad (5)$$

$$NaH + NaAlH_4 \leftrightarrow [Na_2AlH_5] \quad (6)$$

$$NaH + [Na_2AlH_5] \leftrightarrow Na_3AlH_6 \quad (7)$$

$$Na_3AlH_6 \leftrightarrow 3NaH + AlH_3 \quad (8)$$

$$AlH_3 \leftrightarrow Al + 3H \quad (9)$$

$$2H \leftrightarrow H_2 \quad (10)$$

In this reaction pathway, the initial concentration of NaH is limited to low level by the reactions in Eq. (7), which acts as a sink by consuming the NaH. The build up of NaH is enhanced in step 8. The metastable AlH_3 formed in step 9 quickly decomposes into Al and hydrogen atoms (which combine to form hydrogen molecules). In this way we can understand how Al is transported through the system. It is still unclear whether the Na_2AlH_5 formed is an amorphous structure or has a well-defined crystal structure. We discuss the likely structure of Na_2AlH_5 at a later stage in this paper. This pathway nicely explains the mass transport of Al atom by using AlH_3 as the mobile species. However, the most likely decomposition scenario of Na_2AlH_5 is

$$2Na_2AlH_5 \leftrightarrow NaAlH_4 + Na_3AlH_6 \quad (11)$$

which is analogous to the disproportionation of K_2ErF_5 [16] as follows:

$$2K_2ErF_5 \leftrightarrow KErF_4 + K_3ErF_6 \quad (12)$$

With this in mind, Eq. (11) calls for a re-examination of reactions (6), (7) from a thermodynamics perspective.

A second and pragmatic approach to understanding the dynamical details of thermal decomposition of $NaAlH_4$ is to look at the reactions involving NaF–AlF_3 system, which is similar to the NaH–AlH_3 system. It is worth noting that both α-Na_3AlH_6 and α-Na_3AlF_6 have similar crystal structure (monoclinic symmetry, space group $P2_1/n$) and undergo a pressure induced phase transformation to a cubic β-phase (space group $Fm\bar{3}m$), β-Na_3AlH_6 and β-Na_3AlF_6, respectively. Similarly, both α-AlH_3 and α-AlF_3 [17] have a rhombohedral structure (space group $R\bar{3}c$) and both undergo a pressure induce phase transformation to a cubic phase (space group $Pm\bar{3}m$). In the sodium fluoride systems NaF–AlF_3, NaF, AlF_3, Na_3AlF_6 and $Na_5Al_3F_{14}$ [18] exists as stable phases while $NaAlF_4$ is metastable. In particular NaF, Na_3AlF_6 and $Na_5Al_3F_{14}$ occur in nature as villiamunite, cryolite and chiolite, respectively. Another important pointer to the similarity of the crystal structures of alanates and alarides (alumino-fluorides) is that both K_2NaAlH_6 [19] and K_2NaAlF_6 (elpasolite) have cubic symmetry (space group $Fm\bar{3}m$). Of particular interest is the existence of $Na_5Al_3F_{14}$, which is yet to be explored in the NaH–AlH_3 system.

In this work we have examined the two possible pathways: Na_2AlH_5 and $Na_5Al_3H_{14}$. This paper is divided as follows: Section 2 deals with the computational methodology deployed, Section 3 dwells on results and discussion with emphasis on the possible crystal structures of $Na_5Al_3H_{14}$ and Na_2AlH_5, and decomposition pathways of $NaAlH_4$ using Na_2AlH_5 and $Na_5Al_3H_{14}$ as possible intermediate states. Section 4 gives a summary of what is discussed herein.

2. Computational methodology

Geometry optimizations of $Na_5Al_3H_{14}$ and Na_2AlH_5 were done using projector augmented [20] plane-wave implementation in VASP [21]. The Kohn–Sham groundstate is self-consistently determined in an iteration matrix diagonalization scheme of band by band. The calculations used the generalized gradient approximation of Perdew and Wang [22–24](GGA-PW91) to represent electronic-correlation effects for a particular ionic configuration. For all volumes considered the structures were fully optimized using force as well as stress minimization. The ions involved are steadily relaxed towards equilibrium until the Hellman–Feynman forces are minimized to less than 0.02 eV/Å with conjugate gradient algorithm during all relaxation runs. Once the optimized relaxed structure was found, a further local optimization was done by locally relaxing the structure until the Hellman–Feynman forces on the ions were less than 0.005 eV/Å using quasi-Newton algorithm. A convergence of 0.001 meV/atom was placed as a criterion on the self-consistent convergence of the total energy. In all calculations a well-converged plane wave cutoff of 600 eV was used. Brillouin zone integrations were performed using $4 \times 4 \times 4$ k-points for $Na_5Al_3H_{14}$ structures and $6 \times 6 \times 6$ k-points for Na_2AlH_5 structures as per the Monkhorst–Pack grid procedure [25]. The reference configurations for valence electrons used are H($1s^1$), Na($3s^1$) and Al($3s^2 3p^1$). Two different symmetry constrained approaches were used to determine the equilibrium lattice parameters of the structures considered. In the first case for a fixed cell volume of each structure the cell shape and atomic coordinates were fully optimized until the forces were less that 0.02 eV/Å per atom. The structure with the lowest energy was determined by plotting a total energy versus cell-volume curves, equation of state (EoS), for all the structures considered. The obtained energies were fitted to a Murnaghan EoS [26] in order to get the equilibrium volume and minimum energy. The final structure was then determined by optimizing the lattice parameters and atomic positions at this equilibrium volume until the forces on the ions were less than 0.005 eV/Å per atom. In the second instance all the three lattice parameters (cell volume, lattice constants and atomic positions) were simultaneously relaxed with high accuracy.

To obtain the thermodynamic functions, and to check the mechanical stability for these crystals, the harmonic phonons were calculated by a direct ab initio force constant approach implemented by Parlinski [27]. In this method a specific atom is displaced to induce the forces on the surrounding atoms, which are calculated via the Hellmann–Feynman theorem (output from VASP code). The forces are collected to construct the force-constant matrices. Harmonic phonons were obtained from the diagonalization of the dynamical matrices. The internal energy ($E_{(T)}$) was evaluated from the integral of phonon density of state (DOS) as follows:

$$E_{(T)} = \frac{1}{2} r \int_0^\infty \hbar\omega g(\omega) \coth\left(\frac{\hbar\omega}{2k_B T}\right) d\omega \quad (13)$$

where $g(\omega)$ is the phonon DOS, r is the number of degrees of freedom in the unit cell, $\hbar$ is the Planck constant, k_B is the Boltzmann constant and T is temperature. Similar integrals can be applied to calculate the zero-point (ZP) energy, entropy ($S_{(T)}$) and free energy ($F_{(T)}$) [28]. To obtain Gibbs free energy for H_2 gas at elevated temperatures, the free energy at atmospheric pressure is calculated by combining calculated and measured data as

$$G_{(p_0=1\ \mathrm{atm},T)}(H_2) = E_{\mathrm{elec}}(H_2) + E_{\mathrm{zp}}(H_2) + \triangle G_{(T)}(H_2) \quad (14)$$

where $E_{\mathrm{elec}}(H_2)$ is the electronic energy of a H_2 molecule obtained from the total-energy calculations, $E_{\mathrm{zp}}(H_2)$ is the ZP energy of a H_2 molecule obtained from the phonon calculations. $\triangle G_{(T)}(H_2)$ is the temperature-dependent Gibbs free energy with respect to that at 0 K, which can be obtained from the tabulated thermochemical data [29].

3. Results and discussion

3.1. Structure

The crystal structure of $Na_5Al_3H_{14}$ was explored by examining structures of the form $M'_5M_3F_{14}$ (where M' is a monovalent atom and M is a trivalent atom). The structures fall into four space groups ($P4/mnc$, $I4$, $P2_1/n$ and $P4_22_12$). The structures include $Na_5Al_3F_{14}$ ($P4/mnc$), $Na_5Cr_3F_{14}$ ($P2_1/n$), $Na_5Ga_3F_{14}$ ($P2_1/n$), and $Na_5Fe_3F_{14}$($P2_1/n$) and its high temperature phase $Na_5Fe_3F_{14}$ ($P4_22_12$), $Na_5W_3O_9F_5$, $Ca_5Te_3O_{14}$, $NaNd_4Sb_3O_{14}$ and $Na_4Lu(WNb_2)O_9F_5$, which are all in the $P2_1/n$ space group. To the best of our knowledge all structures of the form $M'_5M_3F_{14}$ should fall into one of these four space groups. This gives us the confidence that all the relevant space group geometric modifications of the structure have been taken into account. Among the phases considered the $P4/mnc$ takes the lowest energy, see Fig. 1. Thus, using density functional theory (DFT), $Na_5Al_3H_{14}$ is found to crystallize in the same space group as $Na_5Al_3F_{14}$.

The lowest energy structure of $Na_5Al_3H_{14}$ is that which crystallizes in the space group $P4/mnc$ with two formula units per unit cell. The DFT calculated lattice parameters are $a = 6.769$ and $c = 10.289$ A. A summary of the optimized internal coordinates is presented in Table 1 while the bondlengths and coordinations are presented in Table 2.

Fig. 2 shows how the $Na_5Al_3H_{14}$ crystal looks like when viewed towards the (1 0 0) and (0 0 1) planes.

The structure can be thought of as a slightly distorted perovskite but that is where the similarity ends since the octahedrons in perovskite share corners infinitely in all three dimensions whereas the AlH_6's in this structure share corners infinitely in only two dimensions. Thus the structure forms layers of AlH_6's octahedra as shown in Fig. 2. There are two types of AlH_6 octahedra whose symmetries are different, which form shifted independent $[Al_3H_{14}]_n^{5n-}$ layers perpendicular to the c-axis, Fig. 3. Within the unit cell, a third of the octahedra share four corners and the remaining share only two. The sharing of *cis* two vertices of an octahedra can lead to either a zigzag chain or cyclic molecules. The doubly bridged and tetra-bridged octahedra form a linear chain due to sharing of *trans* vertices and at the same time are involved in a cyclic network of eight octahedra due to sharing of *cis* vertices, Fig. 3.

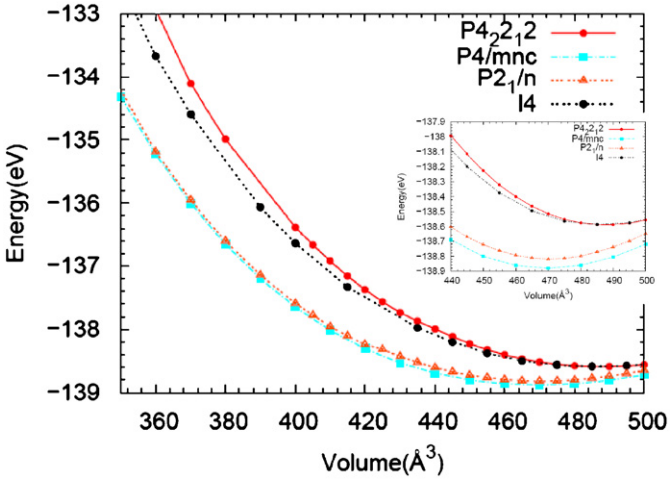

Fig. 1. (Color online) The total energy E (eV) for different lattice volumes of $Na_5Al_3H_{14}$ in different structural modifications and inset is a closer look at the 450–500 region, showing clear energetic difference between the $P4/mnc$ and $P2_1/n$ modifications.

Table 1
Optimized internal coordinates of $Na_5Al_3H_{14}$

Atom	Site	Symmetry	x	y	z
Na_1	2*b*	4/*m*	0	0	0.5
Na_2	8*g*	2	0.2851	0.7851	0.25
Al_1	2*a*	4/*m*	0	0	0
Al_2	4*c*	2/*m*	0	0.5	0
H_1	4*e*	4	0	0	0.1694
H_2	8*h*	*m*	0.7522	0.0731	0
H_3	16*i*	l	0.3207	0.0420	0.6175

Table 2
The interatomic distances and coordination numbers of $Na_5Al_3H_{14}$

Neighbors	Distance (Å)	Coordination
Na–Al (planar)	3.377	8
Na–Na	3.408	8
Al–Al	3.377	4
Na–H	2.221	8

In the first $Al(1)H_6$ octahedron there are four bridging hydrogen atoms and in the second one, $Al(2)H_6$, there are two bridging hydrogen atoms, Fig. 3. The $Al(2)H_6$ octahedra is tilted by 45.69° away from the ideal octahedral structure in perovskite. The Al–H distances are as follows. For the first type, $Al(1)H_6$, $d^{\text{bridge}}_{Al_1-H} = 1.745$ A and $d^{\text{terminal}}_{Al_1-H} = 1.746$ A whereas for the second type, $Al(2)H_6$, $d^{\text{bridge}}_{Al_2-H} = 1.774$ A and $d^{\text{terminal}}_{Al_2-H} = 1.737$ A. Interestingly, in the case of $Al(1)H_6$ the two d_{Al-H} distances are almost equal whereas for $Al(2)H_6$ there is a clear difference. This difference emanates from differing crystalline field the two moieties are subjected to. For $Al(1)H_6$ the Al atom is completely shielded from direct interaction with Na atoms by the H anions while in the case of $Al(2)H_6$ all the terminal H atoms are off planar and hence there is a subtle direct interaction between Na and Al. Within the layers some sodium cations occupy the cavities between the octahedra while the others are in the spaces between the octahedral layers. These two distinct sodium sites give rise to the following coordinations with respect to hydrogen atoms as nearest neighbors. Na(1) (axis symmetry 4/*m*) is 8-fold coordinated whereas Na(2) (local symmetry 2) is 10-fold coordinated. For Na(1) all the Na(1)–H distances are 2.502 Å while for Na(2) the Na(2)–H distances vary from 2.221 to 3.528 Å. By comparison in Na_3AlH_6, Na(1) is 6-fold coordinated and Na(2) is 8-fold coordinated. Further, in Na_3AlH_6 there are two d_{Al-H} distances of 1.783 and 1.773 Å, respectively. In the case of AlH_3, $d_{Al-H} = 1.720$ A. This suggests that the Al–H bonding in AlH_3 is stronger than that in Na_3AlH_6 and $Na_5Al_3H_{14}$.

It appears that the $Al(2)H_6$ is a perfect octahedra with $\theta_{H-Al-H} = 90.0°$, where one H is a bridge atom and the other H is a terminal atom, whereas the $Al(1)H_6$ seems to be a distorted octahedra with $\theta_{H-Al-H} = 92.08°$. By comparison, the octahedra in AlH_3 and Na_3AlH_6 appear to be more distorted with $\theta_{H-Al-H} = 92.35°$ and $\theta_{H-Al-H} = 90.67°$, respectively. The $Na_5Al_3H_{14}$ structure can be best summed up as being made up of alternating layers of corner-sharing AlH_6 octahedra and distorted edge sharing NaH_6^{5-} octahedra.

The crystal structure of Na_2AlH_5 was examined by exploring structures of the form M''_2MF_5 (where M'' is a monovalent atom and M is a trivalent atom). Among the structures considered include: K_2AlF_5 ($P4/mmm$), K_2ErF_5 ($Pc2_1n$), K_2FeF_5 ($Pbcn$), Rb_2CrF_5 ($Pnma$), Tl_2AlF_5 ($C2221$), $(NH_4)_2MnF_5$, K_2SmF_5 [30] and K_2FeF_5 ($Pbam$).

Among these structures the K_2FeF_5 ($Pbam$)-type has the lowest energy. However, a refined optimization followed by vibrational

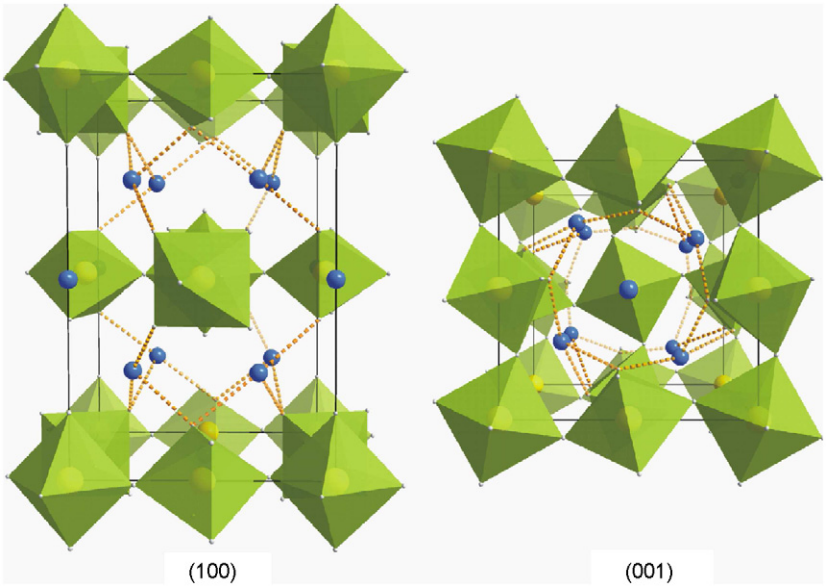

Fig. 2. (Color online) Projections of the $Na_5Al_3H_{14}$ structure. Na atoms are represented by small spheres. The polyhedra represents the AlH_6 moiety.

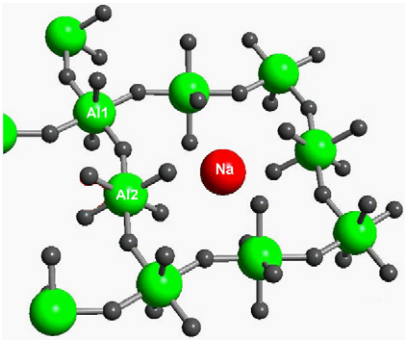

Fig. 3. (Color online) The two types of AlH_6 octahedra, $Al(1)H_6$ and $Al(2)H_6$, in $Na_5Al_3H_{14}$ crystal structure.

analysis at the gamma point showed that the structure is unstable. The instability emanates from the frustrated rotation of the AlH_6 octahedron. However, since we were able to identify only eight possible prototype structures the results on the possible structures of Na_2AlH_5 are not conclusive. For the eight prototype structures of Na_2AlH_5 considered, the structure with the lowest energy (K_2FeF_5(*Pbam*)-type) adopts a zigzag conformation of $[AlH_6]_n^{2n-}$, see Fig. 4. In between the zigzag chains, the Na^+ ions provide the electrostatic stabilization of the lattice.

3.2. Heats of formation/reaction

The heat of formation ΔH_f from the VASP enthalpies of the constituent elements in their standard states were determined as per the following definition:

$$\Delta H_f = H_{Solid} - \sum_a H^{isolated} \quad (15)$$

where a is the different atoms constituting the solid.

Table 3 presents the values of the heats of formation of $NaAlH_4$, Na_3AlH_6, Na_2AlH_5 and $Na_5Al_3H_{14}$. The heat of formation of $Na_5Al_3H_{14}$ from its constituent elements falls in between that of $NaAlH_4$ and Na_3AlH_6.

The heat of formation of $Na_5Al_3H_{14}$ is similar to that of quasi stationary state of Na_2AlH_5 and falls in between that of $NaAlH_4$ and Na_3AlH_6, which implies that both are possible reaction intermediates in the thermal decomposition of $NaAlH_4$. The energetics of $NaAlH_4$ decomposition via the Na_2AlH_5 route are as follows:

$$NaAlH_4 \rightarrow NaH + AlH_3 \quad 36.7\,kJ/mol\,AlH_3 \quad (16)$$

$$NaH + NaAlH_4 \rightarrow [Na_2AlH_5] \quad -5\,kJ/mol \quad (17)$$

$$NaH + [Na_2AlH_5] \rightarrow Na_3AlH_6 \quad -14\,kJ/mol \quad (18)$$

$$Na_3AlH_6 \rightarrow 3NaH + AlH_3 \quad 55\,kJ/mol\,AlH_3 \quad (19)$$

Fig. 5 shows the overall energy cost involved in the Na_2AlH_5 pathway.

It can be seen that Na_3AlH_6 has a local minima in this pathway while the position of Na_2AlH_5 is near a local maxima. This therefore suggests that Na_2AlH_5 is a metastable intermediate and quickly reacts with NaH to form Na_3AlH_6 as was suggested in Ref. [15]. This explains why Na_2AlH_5 is not seen in experiments.

On the other hand, supposing that $Na_5Al_3H_{14}$ exists and is an intermediate in the decomposition pathway of $NaAlH_4$ then one route of forming AlH_3 is via the reaction

$$5NaAlH_4 \rightarrow Na_5Al_3H_{14} + 2AlH_3 \quad (20)$$

This is similar to the disproportionation of the metastable $NaAlF_4$ upon heating:

$$5NaAlF_4 \rightarrow Na_5Al_3F_{14} + 2AlF_3 \quad (21)$$

which takes place at the temperature range of 700–900 K [31].

The $Na_5Al_3H_{14}$ then quickly disproportionates via two possible routes

$$Na_5Al_3H_{14} \rightarrow 5NaH + 3AlH_3 \quad (22)$$

or

$$Na_5Al_3H_{14} \rightarrow \tfrac{5}{3}Na_3AlH_6 + \tfrac{4}{3}AlH_3 \quad (23)$$

Considering the two possible pathways, we can see that route (22) is the back-reaction of the formation of $Na_5Al_3H_{14}$ from NaH and AlH_3 educts. Further, it does not account for the formation of the experimentally observed Na_3AlH_6 phase. In addition, in pathway (22) NaH is formed right at the onset of the decomposition reaction. This contradicts the experimental works of Gross et al. [5] in which it was shown that the $NaAlH_4$, Na_3AlH_6 and NaH are interdependent. This means that low concentrations of NaH

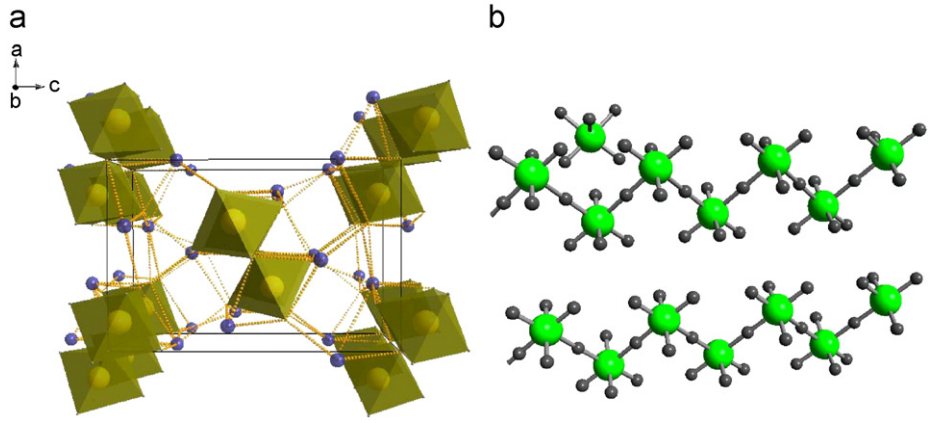

Fig. 4. (a) (Color online) Projections of the Na_2AlH_5 structure. (b) The zigzag nature of the AlH_6 octahedra units in Na_2AlH_5 with the Na atoms removed.

Table 3
Heats of formation for the various complex sodium alanates

Reactants	H_f (kJ/mol H_2)
$Na + Al + 2H_2 \rightarrow NaAlH_4$	−51.0
$5Na + 3Al + 7H_2 \rightarrow Na_5Al_3H_{14}$	−60.0
$2Na + Al + \frac{5}{2}H_2 \rightarrow Na_2AlH_5$	−60.4
$3Na + Al + 3H_2 \rightarrow Na_3AlH_6$	−69.7

Table 4
Heats of reaction for the various complex sodium alanates

Reactants	H_r (kJ/mol AlH_3)
$5NaAlH_4 \rightarrow Na_5Al_3H_{14} + 2AlH_3$	23.9
$Na_5Al_3H_{14} \rightarrow 5NaH + 3AlH_3$	44.8
$Na_5Al_3H_{14} \rightarrow \frac{5}{3}Na_3AlH_6 + \frac{4}{3}AlH_3$	27.6
$Na_3AlH_6 \rightarrow 3NaH + AlH_3$	55.0

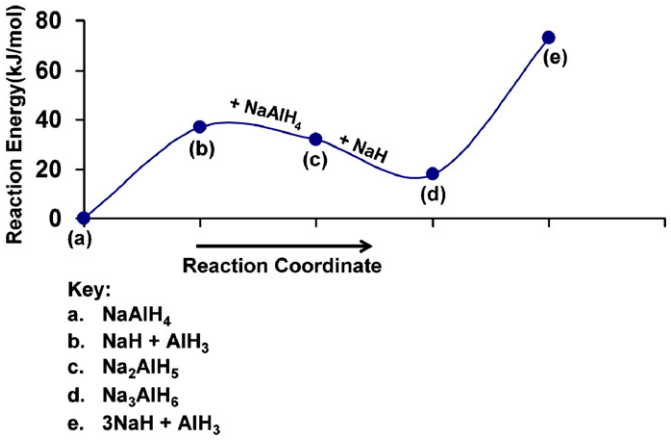

Fig. 5. The energetics of the Na_2AlH_5 pathway.

have to be maintained during the thermal decomposition process until most of the $NaAlH_4$ is used up. Pathway (22) clearly violates this requirement, which leaves the reaction of Eq. (23) as the preferred pathway. The energy cost for disproportionation of $Na_5Al_3H_{14}$ into Na_3AlH_6 and AlH_3, reaction (23), is 27.6 kJ/mol AlH_3. We discuss this later.

With $Na_5Al_3H_{14}$ as the intermediate, the possible reaction pathway is as follows:

$$5NaAlH_4 \leftrightarrow Na_5Al_3H_{14} + 2AlH_3 \quad (24)$$

$$Na_5Al_3H_{14} \leftrightarrow \tfrac{5}{3}Na_3AlH_6 + \tfrac{4}{3}AlH_3 \quad (25)$$

$$Na_3AlH_6 \leftrightarrow 3NaH + AlH_3 \quad (26)$$

$$AlH_3 \leftrightarrow Al + \tfrac{3}{2}H_2 \quad (27)$$

The heats of reaction of the process in Eqs. (24) and (25) are given in Table 4. These energies are consistent with the trend in the thermal decomposition pathway of $NaAlH_4$.

It is interesting to note that the heats of reaction of $NaAlH_4$ to form Na_3AlH_6 and that to form $Na_5Al_3H_{14}$ are very close.

$$5NaAlH_4 \leftrightarrow Na_5Al_3H_{14} + 2AlH_3 \quad 23.9\,kJ/mol \quad (28)$$

$$3NaAlH_4 \leftrightarrow Na_3AlH_6 + 2AlH_3 \quad 25.4\,kJ/mol \quad (29)$$

This suggests that these two processes are competitively similar. However, a better understanding of the two reactions entails computation of Gibbs free energy of formation (product minus reactant, ΔG). The temperature dependent Gibbs free energy can be calculated from

$$G = U + pV - TS \quad (30)$$

$$= E_{elec} + E_T + pV - TS \quad (31)$$

where E_{elec} is the electronic energy and E_T is the internal energy, which is evaluated as follows:

$$E(T) = \frac{1}{2}\hbar r \int_0^\infty \coth\left(\frac{\hbar w}{2k_BT}\right)\omega g(\omega)\,d\omega \quad (32)$$

where $g(\omega)$ is the phonon DOS of the unit cell, r is the number of degrees of freedom in the unit cell, k_B is Boltzmann constant, T is the temperature and $\hbar$ is Planck's constant. The vibrational entropy of the system, $S(T)$, is given by

$$S(T) = rk_B \int_0^{\omega_\infty} g(\omega)\left\{\left(\frac{\hbar}{2k_BT}\right)\left[\coth\left(\frac{\hbar}{2k_BT}\right) - 1\right] - \ln\left[1 - \exp\left(-\frac{\hbar\omega}{k_BT}\right)\right]\right\} d\omega \quad (33)$$

Referring to Eq. (31), usually in the case of solid-state materials the pV term contribution at atmospheric pressure is negligible e.g. for $NaAlH_4$ the value of this term at 300 K is $pV = 4.6 \times 10^{-5}$ eV. Therefore, we can as well approximate G as

$$G = E_{elec} + E_T - TS \quad (34)$$

where H is the enthalpy of the reaction. The above thermodynamic functions are obtained by using the harmonic approximation.

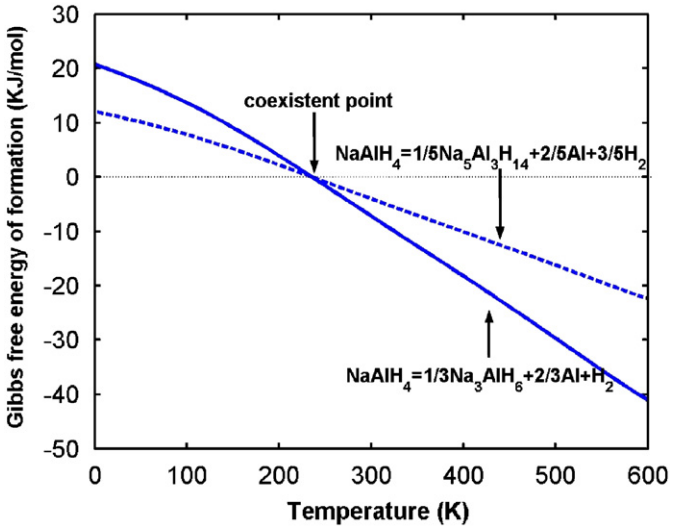

Fig. 6. (Color online) Calculated Gibbs free energy of reactions $NaAlH_4 \rightarrow \frac{1}{5}Na_5Al_3H_{14} + \frac{2}{5}Al + \frac{3}{5}H_2$ and $NaAlH_4 \rightarrow \frac{1}{3}Na_3AlH_6 + \frac{2}{3}Al + H_2$. The reference energies are those of $NaAlH_4$ (denoted by the dotted lines).

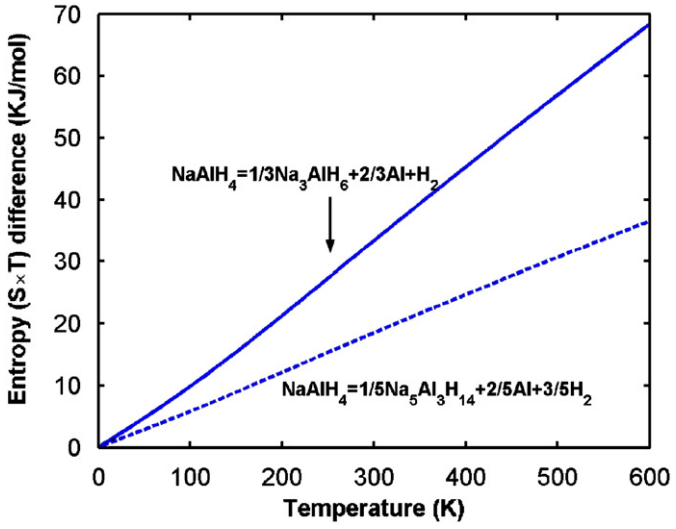

Fig. 7. (Color online) Calculated entropy difference for the reactions $NaAlH_4 \rightarrow \frac{1}{5}Na_5Al_3H_{14} + \frac{2}{5}Al + \frac{3}{5}H_2$ and $NaAlH_4 \rightarrow \frac{1}{3}Na_3AlH_6 + \frac{2}{3}Al + H_2$.

Strictly speaking, reactions (28) and (29) refer to molecular AlH_3, which decomposes into aluminum and hydrogen as shown in reaction (26). To calculate the Gibbs free energies for the two reactions we assume that AlH_3 dissociate into aluminum and hydrogen. Thus the two reactions can be rewritten as

$$NaAlH_4 \rightarrow \tfrac{1}{5}Na_5Al_3H_{14} + \tfrac{2}{5}Al + \tfrac{3}{5}H_2 \quad (35)$$

$$NaAlH_4 \rightarrow \tfrac{1}{3}Na_3AlH_6 + \tfrac{2}{3}Al + H_2 \quad (36)$$

Fig. 6 shows the calculated Gibbs free energy difference for reactions (35) and (36).

The figure shows that before the decomposition of $NaAlH_4$, the product of $(\frac{1}{5}Na_5Al_3H_{14} + \frac{2}{5}Al + \frac{3}{5}H_2)$ is more stable than that of $(\frac{1}{3}Na_3AlH_6 + \frac{2}{3}Al + H_2)$. Even more interesting, there is a coexistent point between these two reactions. This implies that reactions (35) and (36) can be switched. Hence, if we neglect the effect of soft modes (in $Na_5Al_3H_{14}$), then indeed $Na_5Al_3H_{14}$ may be considered as an intermediate state.

Fig. 7 shows the entropy difference (product minus reactant) for the two reactions.

The entropy differences are always positive. This shows that it is the entropy contribution that is the driving force for reactions (35) and (36). The entropy difference for reaction (36) increases at a faster rate than that for reaction (35), which explains why as the temperature increases reaction (36) becomes favored.

$Na_5Al_3H_{14}$ can be synthesized through ball milling of NaH and AlH_3 (amorphous). There are three possible structures that can result from this approach as presented in Table 5 together with their reaction enthalpies.

What one can see in Table 5 is that the three routes have distinct morphological changes that entails bond breaking and formation. Therefore the end product ($NaAlH_4$, Na_3AlH_6 or $Na_5Al_3H_{14}$) might depend on the state/phase of AlH_3 used. AlH_3 is a covalent binary hydride, with polymeric $(AlH_3)n$ forms. Although there are at least seven $(\alpha, \alpha', \beta, \gamma, \delta, \varepsilon, \zeta)$ known non-solvated phases of AlH_3 [32] but only the α, α', β and γ phases are well documented. In calculating the enthalpies of reaction in Table 5 we used the energy of β-AlH_3 polymorph, which was shown by Ke et al. [33] to be the most stable phase of AlH_3. One can deduce in Table 5 that the heat of formation of $Na_5Al_3H_{14}$ from the component hydrides, the process $5NaH + 3AlH_3 \rightarrow Na_5Al_3H_{14}$,

Table 5
Heats of reaction

Reactants	H_r (kJ/mol AlH_3)
$NaH + AlH_3 \rightarrow NaAlH_4$	−36.7
$3NaH + AlH_3 \rightarrow Na_3AlH_6$	−55.1
$5NaH + 3AlH_3 \rightarrow Na_5Al_3H_{14}$	−44.8

is −44.8 kJ/mol AlH_3, which falls between that leading to the formation of $NaAlH_4$ and Na_3AlH_6.

Strictly speaking, the state of AlH_3 in the thermal decompositions of $NaAlH_4$ should be molecular. However, in computing enthalpies of reactions and formations throughout this work the formation enthalpy of crystalline AlH_3 was used for the sake of consistency with Tables (4) and (5). Since the most important quantity here is the energy difference this should not affect the overall energy cost even if the enthalpy values of molecular AlH_3 were to be used.

4. Conclusion

A thermodynamics approach to understanding the reaction pathway of the thermal decomposition of $NaAlH_4$ has been undertaken. The ground state crystal structures of possible intermediates in this reaction pathway, Na_2AlH_5 and $Na_5Al_3H_{14}$, have been explored. $Na_5Al_3H_{14}$ is found to crystallize in the space group $P4/mnc$ with lattice constants $a = 6.769$ A, $c = 10.289$ A and $c/a = 1.52$. It can be thought of as being made up of a distorted and two-dimensional perovskite like network of AlH_6^{3-} and Na^+ units in which both linear and zigzag chains of AlH_6^{3-} octahedra exists. The structure is similar to that of $Na_5Al_3F_{14}$ with the F replaced by H. The decomposition mechanism proceeds as follows:

$$5NaAlH_4 \leftrightarrow Na_5Al_3H_{14} + 2AlH_3 \quad 23.9\,kJ/mol\,AlH_3 \quad (37)$$

$$Na_5Al_3H_{14} \leftrightarrow \tfrac{5}{3}Na_3AlH_6 + \tfrac{4}{3}AlH_3 \quad 27.6\,kJ/mol\,AlH_3 \quad (38)$$

$$Na_3AlH_6 \leftrightarrow 3NaH + AlH_3 \quad 55\,kJ/mol\,AlH_3 \quad (39)$$

$$AlH_3 \leftrightarrow Al + \tfrac{3}{2}H_2 \quad (40)$$

For the case whereby Na_2AlH_5 is an intermediate state the decomposition process is as follows:

$$NaAlH_4 \rightarrow NaH + AlH_3 \quad 36.7\,kJ/mol\,AlH_3 \tag{41}$$

$$NaH + NaAlH_4 \rightarrow [Na_2AlH_5] \quad -5\,kJ/mol \tag{42}$$

$$NaH + [Na_2AlH_5] \rightarrow Na_3AlH_6 \quad -14\,kJ/mol \tag{43}$$

$$Na_3AlH_6 \rightarrow 3NaH + AlH_3 \quad 55\,kJ/mol\,AlH_3 \tag{44}$$

The lowest energy structure of Na_2AlH_5 considered was found to have negative frequencies during vibrational analysis and was therefore taken to be a quasi-stationary state. Based on the relative energies it can be argued that maybe Na_2AlH_5 is an intermediate state but is not observed because it is a quasi-stationary state. These results are consistent with the notion that AlH_3 is an intermediate state during the thermal decomposition process of $NaAlH_4$. The fact that neither Na_2AlH_5 nor $Na_5Al_3H_{14}$ are observed in experiments can be due to the fact that, if they occur during the thermal decomposition of $NaAlH_4$ then, they are quasi-stationary states. In particular the inclusion of $Na_5Al_3H_{14}$ in the decomposition pathway of $NaAlH_4$ nicely explains how the lattice structure of $NaAlH_4$ is disrupted and the mobile alane species are formed.

Acknowledgments

This work is part of the research programs of Advanced Chemical Technologies for Sustainability (ACTS), which is funded by Nederlandse Organisatie voor Wetenschappelijk Onderzoek (NWO). We thanks NSF of China with grant No 10504007.

References

[1] B. Bogdanovic, M. Schwickardi, J. Alloys Compd. 253 (1997) 1–9.
[2] B.C. Hauback, H.W. Brinks, C.M. Jensen, K. Murphy, A.J. Maeland, J. Alloys Compd. 358 (2003) 142–145.
[3] E. Rönnebro, D. Noréus, K. Kadir, A. Reiser, B. Bogdanovic, J. Alloys Compd. 299 (2000) 101–106.
[4] V. Ozolins, E.H. Majzoub, T.J. Udovic, J. Alloys Compd. 375 (2004) 1–10.
[5] J.K. Gross, S. Guthrie, S. Takara, G. Thomas, J. Alloys Compd. 297 (2000) 270–281.
[6] J. Íñiguez, T. Yildirim, T.J. Udovic, M. Sulic, C.M. Jensen, Phys. Rev. B 70 (6) (2004) 060101.
[7] A. Aguayo, D.J. Singh, Phys. Rev. B 69 (15) (2004) 155103.
[8] S.M. Opalka, D.L. Anton, J. Alloys Compd. 356 (2003).
[9] A. Peles, J.A. Alford, Z. Ma, L. Yang, M.Y. Chou, Phys. Rev. B 70 (16) (2004) 165105.
[10] E.H. Majzoub, K.F. McCarty, V. Ozoliņš, Phys. Rev. B 71 (2) (2005) 024118.
[11] Q.J. Fu, A.J. Ramirez-Cuesta, S.C. Tsang, J. Phys. Chem. B 110 (2006) 711–715.
[12] S. Chaudhuri, J.T. Muckerman, J. Phys. Chem. B Lett. 109 (2005) 6952–6957.
[13] E.C. Ashby, P. Kobetz, Inorg. Chem. 5 (1966) 1615.
[14] A.E. Finholt, G.D. Barbaras, G.K. Barbaras, G. Urry, T. Wartik, H.I. Schlesinger, J. Inorg. Nucl. Chem. 1 (1955) 317.
[15] R.T. Walters, J.H. Scogin, J. Alloys Compd. 379 (2004) 135.
[16] N.V. Podberezskaya, S.V. Borisov, V.I. Alekseev, M.N. Tseitlin, Kh.M. Kurbanov, J. Struct. Chem. 23 (1982) 158–160.
[17] R. Hoppe, D. Kissel, J. Flourine Chem. 24 (1984) 327–340.
[18] C. Jacoboni, A. Leble, J.J. Rousseau, J. Solid State Chem. 36 (1981) 297–304.
[19] M.H. Sorby, H.W. Brinks, A. Fossdal, K. Thorshaug, B.C. Hauback, J. Alloys Compd. 415 (2006) 284–287.
[20] P.E. Blöchl, Phys. Rev. B 50 (1994) 17953–17979.
[21] G. Kresse, J. Furthmüller, Phys. Rev. B 54 (1996) 11169–11186.
[22] J.P. Perdew, J.A. Chevary, S.H. Vosko, K.A. Jackson, M.R. Pederson, D.J. Singh, C. Fiolhais, Phys. Rev. B 46 (1992) 6671–6687.
[23] J.P. Perdew, K. Burke, Y. Wang, Phys. Rev. B 54 (1996) 16533–16539.
[24] J.P. Perdew, K. Burke, M. Ernzerhof, Phys. Rev. Lett. 77 (1996) 3865–3868.
[25] H.J. Monkhorst, J.D. Pack, Phys. Rev. B 13 (1976) 5188–5192.
[26] F.D. Murnaghan, Proc. Natl. Acad. Sci. USA 30 (1944) 244.
[27] K. Parlinski, Software, PHONON, Institute of Nuclear Physics, Crakow, 2005.
[28] A.A. Maradudin, E.W. Montroll, G.H. Weiss, I.P. Ipatova, Theory of lattice dynamics in the harmonic approximation, in: Solid State Physics Supplement, vol. 3, Academic Press, New York, 1971.
[29] D.R. Stull, H. Prophet, JANAF Thermodynamical Tables, second ed., U.S. National Bureau of Standards, Washington, DC, 1971.
[30] R.I. Bochkova, Y.N. Saf'yanov, É.A. Kuz'min, N.V. Belov, Sov. Phys. Dokl. 18 (1974) 575.
[31] M. Bruno, O. Herstad, J.L. Holm, J. Therm. Anal. Calorimetry 56 (1999) 51–57.
[32] J. Graetz, M. James Reilly, J. Alloys Compd. 424 (2006) 262–265.
[33] X. Ke, A. Kuwabara, I. Tanaka, Phys. Rev. B 71 (18) (2005) 184107.